ISA Transactions 159 (2025) 364–374

Contents lists available at ScienceDirect

ISA Transactions

journal homepage: www.elsevier.com/locate/isatrans

Research article

Modified inverted pendulum on a cart system with four-bar mechanism

Sinan Basaran

Bilecik Seyh Edebali University, Faculty of Engineering, Department of Mechanical Engineering, TR, Bilecik 11210, Türkiye

ARTICLE INFO

Keywords:
Inverted pendulum on a cart
Four-bar mechanism
Backstepping control design

ABSTRACT

In this study, the inverted pendulum on cart system, classic problem of control theory has been modified and an experimental control design has been proposed to maintain balance of a four-bar mechanism instead of a traditional pendulum rod system. Both the inverted pendulum on cart system and the four-bar mechanism are commonly used systems that have been the subject of many control theory problems. Therefore, the combination of these two widely studied systems, which is the focus of this research paper, could very well be integrated for various practical problems such as Segway transportation systems, robotic applications, and rocket guidance systems. With this motivation the modified system has been designated as the "four-bar on a cart system", and dynamic equations of motion have been obtained using the Lagrange method. Furthermore, the performance of the system has been validated through an established experimental setup, and the experimental results for a Lyapunov type backstepping controller are presented. The utilization of a four-bar mechanism instead of a pendulum rod has led to greater challenges in the derivation of the motion of equation due to the additional link position variables in the system. However, despite the modifications on the system, the total degrees of freedom remain unchanged, and the system continues to exhibit dynamic behavior similar to inverted pendulum on cart system. For the completeness of the proposed topic, the inverted pendulum on cart system was initially investigated in this study, and its experimental results were presented. Subsequently, the focus shifted to the four-bar on a cart system.

1. Introduction

Inverted pendulum systems consist of a pendulum where its center of mass is located above the pivot point. The pendulum rod is prone to falling due to their inherently unstable nature without any implementation of a control design on the dynamic system. To make transition from unbalanced state of the pendulum system into a balanced state, control systems that facilitate linear and rotational movements around the pivot point must be employed on the structure. Inverted pendulum on cart system (IPCS) is characterized by having two degrees of freedom, in which the cart moves horizontally, and the pendulum rod can freely rotate around the pivot joint. IPCS has been extensively studied and various control designs have been developed by numerous researchers or research groups, considering it as a fundamental benchmark problem [1–4]. The structure of inverted pendulum systems can be encountered in various engineering systems such as robotic application [5,6]. It can serve as a base for wheeled mobile platforms and mobile robot systems [7,8]. This study focuses on the modification of the classical inverted pendulum system to use for a four-bar mechanism. The four-bar mechanism is the most fundamental and well-known problem in mechanical engineering. The four-bar mechanism is a simple movable closed-chain linkage. It is formed by connecting four links to each other through four revolute joints. The four-bar mechanism is a versatile system that can be used for many mechanical purposes, primarily to convert rotational motion into reciprocating motion. It is a common mechanism chain found in various structures such as compressors, steering mechanisms, bicycles, and other engineering equipment. Researchers conduct various kinematic analyses on the four-bar mechanism [9], and structures utilizing this mechanism can be found in various industrial applications. Zhao et al. worked on the design of a flapping wing robot in their study and proposes a unified design formula for planar four-bar mechanism [10]. Aoustin and Hamon studied the performance of a planar two-legged robot equipped with cross four-bar linkages in their research for a more realistic walking gait [11]. Another research team proposed a robotic hand structure with a four-bar linkage mechanism to overcome the limitations associated with the use of cable-driven mechanisms [12].

Looking at academic and industrial studies, it is evident that both the inverted pendulum system and the four-bar mechanism have been the subjects of great research efforts. Specifically, achieving a stable inverted pendulum mechanism without a control design is not possible. Therefore, diverse studies on the classic pendulum system have been

E-mail address: sinan.basaran@bilecik.edu.tr.

https://doi.org/10.1016/j.isatra.2025.02.014
Received 6 February 2024; Received in revised form 25 July 2024; Accepted 12 February 2025
Available online 13 February 2025

Nomenclature and Abbreviation

b_{fb}	damping coefficient at the four-bar mechanism joints
b_m	damping coefficient of the mobile platform system
b_p	damping coefficient at the pendulum pivot point
F	force acting on mobile platform due to DC motor
J_{eq}	equivalent moment of inertia
J_{dc}	motor moment of inertia
k_b	motor back emf constant
k_{dc}	gear ratio associated with the motor
k_t	motor torque constant
r_{dc}	motor pinion radius
R_m	motor armature resistance
V_{dc}	system control voltage
ε	efficiency of the gearbox
FBCS	four-bar on a cart system
IC	instant centers of velocity point
IPCS	inverted pendulum on cart system

conducted to make this problem more complex, leading to the emergence of unique structures. To this end, Francoa et al., examine the balance control problem for flexible inverted-pendulum systems and investigate the relationship between system parameters and robustness under disturbance effects [13]. After accepting the assumption of the elasticity of the pendulum rod, one of the most intriguing subjects is the structures that use two pendulum rods simultaneously. In another study, a decentralized adaptive control scheme was applied to a system consisting of two inverted pendulums mounted on separate carts connected by a spring. A challenging problem was presented to demonstrate the effectiveness of the proposed controller [14]. A single cart with two independent inverted pendulum rods, is analyzed by Lundherg and Roberge [15] and they compared to the single-inverted-pendulum system using classical linear methods of proposed dual rod system. On the other hand, Tsai and Shen proposed a dual-pendulum system, where two independent inverted pendulum rods are connected to a rigid body at their ends, enabling synchronized operation on a dual cart system [16].

In this study, the inverted pendulum system has been modified using a four-bar mechanism in a way that has not been encountered in the literature previously. The novelty of the research comes from the main objective which is to maintain the balance of a four-bar mechanism instead of a rod in the inverted pendulum system. Therefore, the four-bar on a cart system (FBCS), inspired by the inverted pendulum system, can find applications in balance systems with joints that facilitate movement kinematically. This could be in transportation systems like the Segway or a system where two separate rockets are connected with joints to move together. In a classical inverted pendulum system, maintaining balance is achieved by controlling the movement of a rod pivoting around 90 degrees on a mobile platform through a motor. However, the suggested four-bar on a cart mechanism has its equilibrium position changing depending on the angular position of link-2, link-3, or link-4, excluding the fixed link (link-1) in the mechanism. To determine the correct balance angle, the center of mass of the four-bar mechanism and the instant centers of velocity points have been calculated and utilized. Furthermore, due to the high number of position variables in the four-bar mechanism, obtaining the dynamic equation of motion of the proposed system has required extensive effort. However, by utilizing the Freudenstein equation and expressing the position of link-3 and link-4 as a function of the positions of link-2, the equations of motion have been derived. A study involving the Lagrangian dynamics of only the four-bar mechanism has been conducted as outlined in the reference [17]. However, considering a whole system with a moving platform, for the first time the dynamics of the FBCS with two degrees of freedom have been introduced in this study. Before presenting the control design and experimental studies for the FBCS, the work inspired by the IPCS was discussed in the article. Although the proposed system has dynamic equations in closed form similar to the inverted pendulum system, obtaining its dynamics is challenging. A general overview of the literature shows that many different control algorithms have been applied to the inverted pendulum system. Ebrahim and Murphy's studies have demonstrated that the backstepping control design method is effective in synthesizing an asymptotically stable control system for the nonlinear dynamics of the inverted pendulum system [18]. The inverted pendulum system on a wheeled mobile platform, controlled using the backstepping controller, has shown superior results for larger initial angle conditions, as demonstrated in the simulation results discussed in the previous work [19]. In another study, a different control synthesis was used to extend the application to underactuated mechanical systems. Researchers were achieved asymptotic stability for the inherently unstable inverted pendulum system [20]. In this study, instead of a pendulum rod, a four-bar mechanism is used, and the control performance of a system with different link angles, as opposed to a fixed rod, is experimentally demonstrated using a well-known, and recognized Lyapunov-based controller.

The main contribution of this study is the adaptation of the four-bar mechanism, which typically converts circular motion to reciprocating motion and is usually treated as a kinematic problem, to the inverted pendulum system as a dynamic control problem. Consequently, this study provides a framework that can serve as a benchmark problem for various applications, including mechanical linkages, balance systems, Segway transport systems, robotic applications, rocket launches, structural systems, and the simulation of human posture. Therefore, the four-bar on cart system, inspired by the inverted pendulum system, can find applications in various systems with joints that facilitate movement kinematically. Furthermore, it is evident that the conventional inverted pendulum system's equilibrium position occurs when the pendulum rod is vertical, or at a right angle of $\theta = 90^{\circ}$. However, the equilibrium position of the four-bar mechanism depends on the system's center of mass and the instant centres of velocity point (IC). Therefore, the equilibrium position varies based on the lengths of the chosen links, as explained in Section 3.

The content of this study is structured as follows: Before presenting the FBCS, the classical IPCS is introduced in Section 2. In Section 3, the dynamic equations of the FBCS inspired by the IPCS were obtained using the Lagrange method. The equations of motion for both systems are obtained in a similar closed-form structure. In Section 4, Lyapunov-based Backstepping control design has been separately transferred for both systems. Following that, experimental studies conducted for both systems and the obtained results are shared in a similar manner. Finally, a conclusion is drawn.

2. Dynamics of the inverted pendulum on a cart system

In this study a FBCS, inspired by the IPCS, is proposed. To convey the similarity of the dynamics of the proposed FBCS to the IPCS, this section starts by establishing the classical dynamic model of the problem. Fig. 1 illustrates the inverted pendulum system schematically. The system is composed of a rod situated on a movable platform. The IPCS has been the subject of numerous studies in literature. Detailed dynamic models of this system have been developed and applied in various control studies [21–26]. The total kinetic energy of the system consists of both the translational and rotational kinetic energies originating from both the cart and the pendulum.

The first equation of motion, resulting from the translational movement of the cart, is given below:

$$\left(J_{eq}+m\right)\ddot{x}-ml\cos(\theta)\ddot{\theta}+ml\sin(\theta)\dot{\theta}^{2}=F-b_m\dot{x}. \tag{1}$$

Similarly, the rotational equation of motion of the system is as follows:

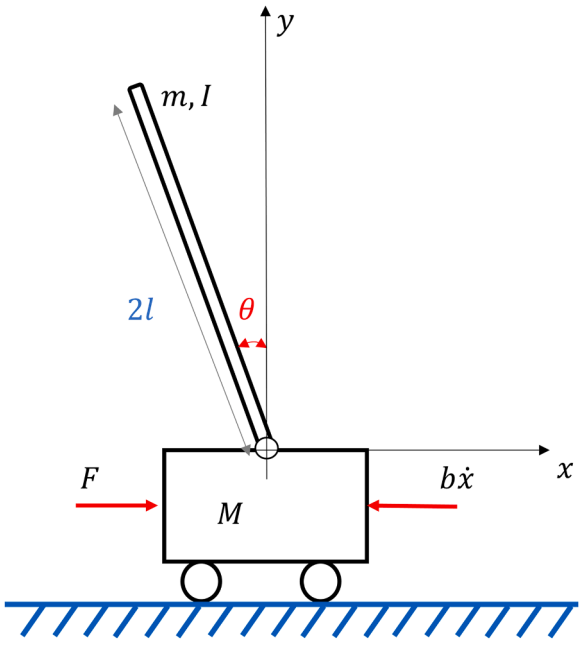

Fig. 1. IPCS schematic view.

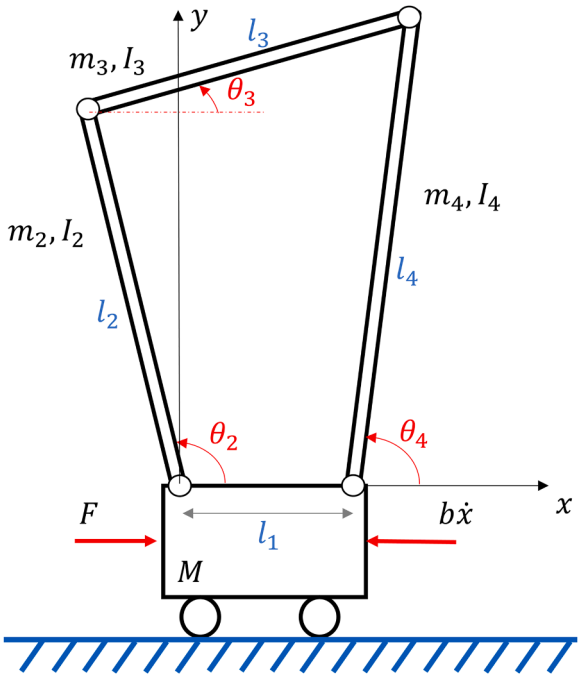

Fig. 2. Modified IPCS with four-bar mechanism.

$$(J_{eq}+ml^2)\ddot{\theta}-mlcos(\theta)\ddot{x}-mglsin(\theta)=-b_p\dot{\theta}. \tag{2}$$

Here, J_{eq} represents the equivalent moment of inertia as given below:

$$J_{eq}=M+\frac{\varepsilon k_{dc}^2 J_{dc}}{r_{dc}^2}. \tag{3}$$

In these equations, k_{dc} represents the gear ratio associated with the DC motor, ε is the efficiency of the gearbox, J_{dc} denotes the motor's moment of inertia, r_{dc} represents the motor pinion radius, b_m represents the equivalent damping coefficient of the mobile platform system, F represent the force acting on mobile platform due to DC motor and b_p represents the damping coefficient at the pendulum pivot point. The equation below can be used to compute the force expression in Eq. (1) in terms of motor control voltage.

$$F=\frac{k_t V_{dc} r_{dc}-k_t k_b \dot{x}}{R_m r_{dc}} \tag{4}$$

here, k_t represents the dc motor torque constant, k_b represents dc motor back emf constant, R_m represents dc motor armature resistance, and V_{dc} represents system control voltage. To eliminate dynamic coupling expressions in the motion equations, the $\ddot{x}$ term from Eq. (1) is extracted and substituted into Eq. (2). Similarly, the $\ddot{\theta}$ term can be extracted from Eq. (2) and substituted into Eq. (1), and with the help of Eqs. (3) and (4), the equations of motion of the system can be transformed into matrix format.

here, $J_T=J_{eq}J_p+mJ_p+ml^2J_{eq}$ has been defined as the simplification term. The equation in matrix form can be written in a closed form as follows:

$$\boldsymbol{M}(\theta)\ddot{\boldsymbol{q}}+\boldsymbol{C}(\theta,\dot{\theta})\dot{\boldsymbol{q}}+\boldsymbol{G}(\theta)=\boldsymbol{F}V_{dc}. \tag{6}$$

3. Dynamics of the four-bar on a cart system

In this study, the main objective is to maintain the balance of a four-bar mechanism instead of a pendulum rod in the IPCS. The schematic diagram in Fig. 2 shows a modified system with a four-bar mechanism. Through the encoder attached to the joint between link-1 and 2 of four-bar mechanism, the instantaneous angle $\theta_2(t)$ of the mechanism is measured in real-time. The instant center of velocity is a point that has the same instantaneous velocity at each body. In a mechanism, instant center velocity points are determined depending on the number of links of the mechanism. According to Kennedy's rule [27] when three bodies move relative to one another, they have three instant centers lying on the same straight line. The total instant centers of velocity in a mechanism can be determined using the following formulation.

$$Number\ of\ IC=\frac{n(n-1)}{2} \tag{7}$$

$$\begin{bmatrix} \frac{-m^2l^2cos^2(\theta)+J_T+m^2l^2}{cos(\theta)(J_{eq}ml+m^2l)} & 0 \\ 0 & \frac{m^2l^2cos^2(\theta)+J_T+m^2l^2}{cos(\theta)(J_pml+m^2l^3)} \end{bmatrix}\begin{bmatrix}\ddot{\theta}\\ \ddot{x}\end{bmatrix}+\begin{bmatrix} \frac{m^2l^2sin(\theta)cos(\theta)\dot{\theta}+b_p(J_{eq}+m)}{(J_{eq}+m)mlcos(\theta)} & \frac{b_{eq}R_mr^2+k_tk_b}{(J_{eq}+m)R_mr^2} \\ \frac{b_pcos(\theta)+sin(\theta)(J_p+ml^2)\dot{\theta}}{(J_p+ml^2)cos(\theta)} & \frac{b_{eq}R_mr^2+k_tk_b}{mlcos(\theta)R_mr^2} \end{bmatrix}\begin{bmatrix}\dot{\theta}\\ \dot{x}\end{bmatrix}+\begin{bmatrix} -\frac{gsin(\theta)}{cos(\theta)} \\ -\frac{mglsin(\theta)}{(J_p+ml^2)} \end{bmatrix}$$
$$=\begin{bmatrix}\frac{k_t}{(J_{eq}+m)R_mr}\\ \frac{k_t}{mlcos(\theta)R_mr}\end{bmatrix}V_{dc} \tag{5}$$

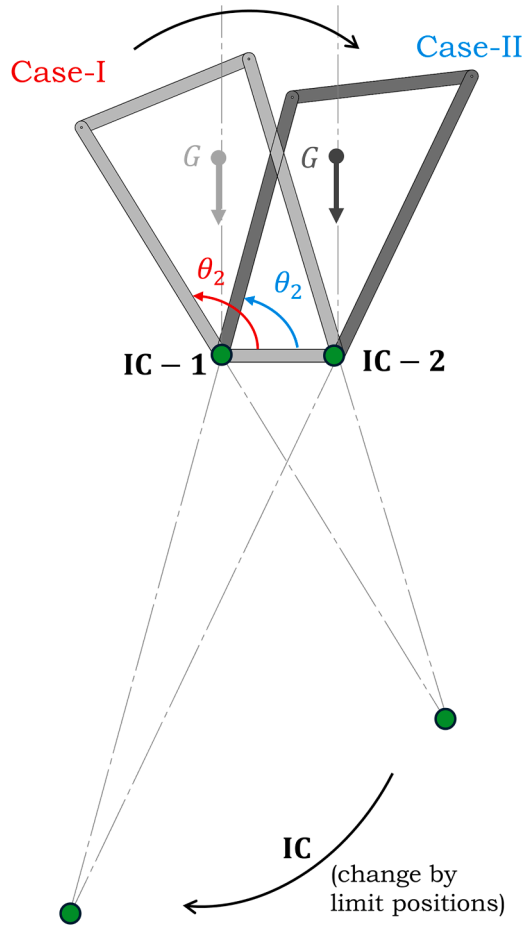

Fig. 3. The relationship between the mechanism's center of mass and the instant center of velocity point.

where, n is the total link number of the mechanism. Hence, in a four-bar mechanism, there are a total of six IC points.

The correlation between the mechanism's center of mass and the IC points varies depending on the mechanism's instant position. As can be seen in Fig. 3, to maintain the balance of the mechanism, the center of mass should be somewhere in between the rotation centers IC-1 and IC-2. Thus, two different cases, considered as the lower and upper limits of the system, are presented in Fig. 3. It is evident that the equilibrium position of the mechanism will be between $\theta_2 = 74.7^{\circ}$ and $\theta_2 = 121.5^{\circ}$ degrees. As the mechanism moves clockwise, as shown in Fig. 3, the center of mass also moves clockwise. Similarly, the IC point moves clockwise and coincides with the center of mass along the same line at certain degrees. In Fig. 4, all IC points of the four-bar mechanism used in experimental studies are shown. In the figure, the green circles represent the six instant centers of velocity points of the mechanism in total. Additionally, the red circle in the figure represents the center of mass position of the four-bar mechanism.

The main point addressed in this study is the determination of the equilibrium position of the four-bar mechanism. Conventionally, in the inverted pendulum system, the equilibrium position is around the vertical position of the rod, where $\theta = 90^{\circ}$.

In the proposed four-bar mechanism, the equilibrium position has been determined using the IC point. The position where the center of mass coincides with the IC center, as shown in the figure, has been identified as the equilibrium position. This position has been determined through a computer aided design (CAD) program by inputting the material information of the four-bar mechanism. At $\theta_2 = 96.5^{\circ}$ degrees, the center of mass of the mechanism intersects with the IC point along the same line. Therefore, in this position, the gravitational force acts as a destabilizing input, causing the system to rotate either to the right or to the left.

In a previous section, the equations of motion of the inverted pendulum system were presented. In this section, the Lagrange method is used to obtain the motion equations of the modified inverted pendulum system for the four-bar mechanism. Despite the complexity introduced by using a four-bar mechanism instead of a simple rod, the total degrees of freedom of the system remain unchanged. In the inverted pendulum system, control is typically conducted around $\theta = 0^{\circ}$ (a right angle $\theta = 90^{\circ}$), where the rod is vertical. In the proposed system, control is carried out around $\theta_2 = 96.5^{\circ}$ degrees. To derive the motion equations, it is necessary to know the angles of the links of the four-bar mechanism, namely θ_2, θ_3, and θ_4. The position of θ_2 is read by the encoder and used in the closed-loop control system design. The angles θ_3 and θ_4 can be expressed in terms of θ_2, as they are dependent on it. Various methods, including the Freudenstein method [28], are employed for position analysis of the four-bar mechanism. This method is preferred for obtaining loop closure equations in mechanisms or structures with closed chains, such as robotic arms [29,30]. The fundamental goal here is to express the unknown angles (θ_3, θ_4) of the mechanism's links in terms of the known θ_2 and determine θ_2 as the generalized coordinate of the mechanism. We can start the calculations of unknown angles by defining the loop closure equations of four-bar mechanism, as illustrated on Fig. 2.

$$l_3\cos(\theta_3) = l_1 + l_4\cos(\theta_4) - l_2\cos(\theta_2),$$

$$l_3\sin(\theta_3) = l_4\sin(\theta_4) - l_2\sin(\theta_2). \tag{8}$$

The sum of the squares of these loop closure equations can be defined as:

$$f_1\sin(\theta_4) + f_2\cos(\theta_4) + f_3 = 0 \tag{9}$$

where f_1, f_2, and f_3 can be defined as a function of θ_2.

$$f_1 = -2l_2l_4\sin(\theta_2),$$

$$f_2 = 2l_4(l_1 - l_2\sin(\theta_2)),$$

$$f_3 = l_1^2 + l_2^2 - l_3^2 + l_4^2 - 2l_1l_2\cos(\theta_2). \tag{10}$$

Let's define the T variable,

$$T = \tan\frac{\theta_4}{2}, \tag{11}$$

and trigonometric relations to solve the Freudenstein equation defined in Eq. (8).

$$\sin(\theta_4) = \frac{2T}{1+T^2},$$

$$\cos(\theta_4) = \frac{1-T^2}{1+T^2}. \tag{12}$$

After trigonometric relations are written into the Eq. (8) solvable quadratic equation which is the function of the T is obtained.

$$T^2(f_3 - f_2) + 2Tf_1 + f_2 + f_3 = 0. \tag{13}$$

The solution of the equation can be written as follows:

$$T = \frac{-f_1 \mp \sqrt{f_1^2 + f_2^2 - f_3^2}}{f_3 - f_2}. \tag{14}$$

With the help of Eq. (11), the unknown θ_4 angle in the four-bar mechanism is obtained.

$$\theta_4 = 2\tan^{-1}\left(\frac{-f_1 \mp \sqrt{f_1^2 + f_2^2 - f_3^2}}{f_3 - f_2}\right). \tag{15}$$

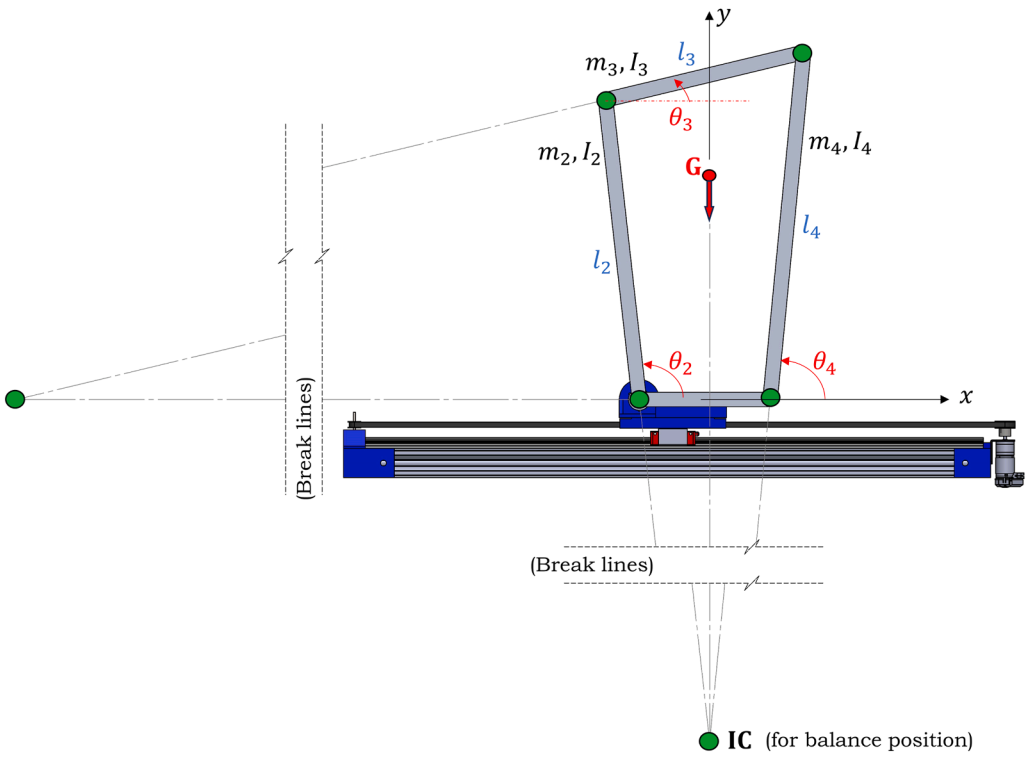

Fig. 4. The position where the instant center (IC) of velocity of the mechanism coincides with the center of mass (G).

Here the plus or minus sign refers to two different configurations of the four-bar mechanism. The other unknown θ_3 angle can be obtained with the help of Eq. (8).

$$\theta_3 = \tan^{-1}\left(\frac{l_4\sin(\theta_4) - l_2\sin(\theta_2)}{l_1 + l_4\cos(\theta_4) - l_2\cos(\theta_2)}\right). \tag{16}$$

By solving the Freudenstein equation, the θ_3 and θ_4 positions of the four-bar mechanism, which has a single degree of freedom defined by θ_2, were obtained in terms of the θ_2 function.

To derive the equations of motion for the proposed system, firstly we should define the total kinetic energy (T_{fb}) expression for both translational and rotational motion.

$$T_{fb} = \frac{1}{2}\left(m_2 v_2^2 + I_2\dot{\theta}_2^2\right) + \frac{1}{2}\left(m_3 v_3^2 + I_3\dot{\theta}_3^2\right) + \frac{1}{2}\left(m_4 v_4^2 + I_4\dot{\theta}_4^2\right). \tag{17}$$

The translational velocities in the equation can be defined as follows:

$$v_2^2 = \dot{x}^2 + \frac{l_2^2}{4}\dot{\theta}_2^2 - l_2\sin(\theta_2)\dot{\theta}_2\dot{x}, \tag{18}$$

$$v_3^2 = \dot{x}^2 + l_2^2\dot{\theta}_2^2 + \frac{l_3^2}{4}\dot{\theta}_3^2 - 2l_2\sin(\theta_2)\dot{\theta}_2\dot{x} - l_3\sin(\theta_3)\dot{\theta}_3\dot{x} + \dot{\theta}_2\dot{\theta}_3\cos(\theta_2 - \theta_3)l_2l_3, \tag{19}$$

$$v_4^2 = \dot{x}^2 + \frac{l_4^2}{4}\dot{\theta}_4^2 - l_4\sin(\theta_4)\dot{\theta}_4\dot{x}. \tag{20}$$

In the mechanism, θ_3 and θ_4 angles are stated as a function of θ_2, and similarly, $\dot{\theta}_3$ and $\dot{\theta}_4$ velocities should be expressed depending on $\dot{\theta}_2$. For this purpose, it is necessary to take the derivative of the loop closure equation defined in Eq. (8). By performing the necessary operations in the equation, the velocities can be obtained as a function of $\dot{\theta}_2$ as follows:

$$\begin{bmatrix}\dot{\theta}_3\\ \dot{\theta}_4\end{bmatrix} = \begin{bmatrix}\frac{l_2\sin(\theta_2-\theta_4)}{l_3\sin(\theta_3-\theta_4)}\\ \frac{l_2\sin(\theta_2-\theta_3)}{l_4\sin(\theta_3-\theta_4)}\end{bmatrix}\dot{\theta}_2 = \begin{bmatrix}D_1(\theta_2,\theta_3,\theta_4)\\ D_2(\theta_2,\theta_3,\theta_4)\end{bmatrix}\dot{\theta}_2 = \begin{bmatrix}\frac{\partial\theta_3}{\partial\theta_2}\\ \frac{\partial\theta_4}{\partial\theta_2}\end{bmatrix}\dot{\theta}_2. \tag{21}$$

Here, D_1 and D_2 are terms, which are function of θ_2, θ_3, and θ_4, are introduced to simplify the expression in the future operations. The general moment of inertia of a link of the mechanism can be defined as follows:

$$I_i = \frac{1}{12}m_i l_i^2, \quad i = 2,3,4. \tag{22}$$

Considering the equivalent kinetic energy of mobile platform (T_m), and kinetic energy of the four-bar mechanism (T_{fb}), the total kinetic energy (T) of the modified system can be expressed as follows:

$$T = T_m + T_{fb}. \tag{23}$$

After the necessary velocity terms are written, the explicit version of the kinetic energy equation can be obtained in the following form.

$$\begin{aligned} T = {} & \left(\frac{m_2l_2^2 + 4m_3l_2^2 + 4I_2}{8}\right)\dot{\theta}_2^2 + \left(\frac{m_3l_3^2 + 4I_3}{8}\right)\dot{\theta}_3^2 + \left(\frac{m_4l_4^2 + 4I_4}{8}\right)\dot{\theta}_4^2 \\ & + \left(\frac{J_{eq} + m_2 + m_3 + m_4}{2}\right)\dot{x}^2 - \left(\frac{(m_2 + 2m_3)l_2}{2}\right)\sin(\theta_2)\dot{\theta}_2\dot{x} \\ & - \left(\frac{m_3l_3}{2}\right)\sin(\theta_3)\dot{\theta}_3\dot{x} - \left(\frac{m_4l_4}{2}\right)\sin(\theta_4)\dot{\theta}_4\dot{x} \\ & + \left(\frac{m_3l_2l_3}{2}\right)\cos(\theta_2 - \theta_3)\dot{\theta}_2\theta \end{aligned} \tag{24}$$

The potential energy originates from the links of the mechanism can be defined as follows:

$$U = m_2g\frac{l_2}{2}\sin(\theta_2) + m_3g\left(l_2\sin(\theta_2) + \frac{l_3}{2}\sin(\theta_3)\right) + m_4g\frac{l_4}{2}\sin(\theta_4). \tag{25}$$

Note that the total kinetic and potential energy terms defined in Eqs. (24) and (25) respectively for the modified system can be expressed in terms of the generalized coordinates of the system, x and θ_2. The Lagrangian expression can be defined by $\mathscr{L} = T - U$ as the difference between kinetic and potential energy for proposed system.

$$\mathscr{L} = P_1\dot{\theta}_2^2 + P_2\dot{\theta}_3^2 + P_3\dot{\theta}_4^2 + P_4\dot{x}^2 - P_5\dot{\theta}_2\dot{x} - P_6\dot{\theta}_3\dot{x} - P_7\dot{\theta}_4\dot{x} + P_8P_9\dot{\theta}_2\dot{\theta}_3 - P_{10} \tag{26}$$

where $P_1 = \left(m_2l_2^2 + 4m_3l_2^2 + 4I_2\right)/8$, $P_2 = \left(m_3l_3^2 + 4I_3\right)/8$, $P_3 = \left(m_4l_4^2 + 4I_4\right)/8$, $P_4 = \left(J_{eq} + m_2 + m_3 + m_4\right)/2$, $P_5(\theta_2) = \sin(\theta_2)(m_2 + 2m_3)l_2/2$, $P_6(\theta_3) = \sin(\theta_3)m_3l_3/2$, $P_7(\theta_4) = \sin(\theta_4)m_4l_4/2$, $P_8 = (m_3l_2l_3)/2$, $P_9(\theta_2, \theta_3) = \cos(\theta_2 - \theta_3)$, and $P_{10}(\theta_2, \theta_3, \theta_4) = U$ are constant terms and functions depending on mechanism link angles.

The Lagrange equation defined below can be used to obtain the first dynamic equation of the system.

$$\frac{d}{dt}\left(\frac{\partial\mathscr{L}}{\partial\dot{\rho}_i}\right) - \frac{\partial\mathscr{L}}{\partial\rho_i} = Q_i, \quad i = 1, 2. \tag{27}$$

Here, ρ_i represents the generalized coordinates of the system and Q_i represents the generalized external forces acting on the system as defined below:

$$\boldsymbol{\rho} = \begin{bmatrix} x \\ \theta_2 \end{bmatrix}, \tag{28}$$

$$\boldsymbol{Q} = \begin{bmatrix} F - b_m\dot{x} \\ -b_{fb}\dot{\theta}_2 \end{bmatrix}. \tag{29}$$

Where b_{fb} represents the equivalent damping coefficient for revolute joints oriented from all links of the four-bar mechanism. Note that, the damping originating from each link of the four-bar mechanism needs to be added to the equation, but to simplify the equation of motion, the equivalent b_{fb} is considered for the entire system. As a result of the Lagrange equation, with the small angle approximation ($\sin(\theta) \approx \theta$, $\cos(\theta) \approx 1$) and the force-voltage Eq. (4), the equation of motion of the FBCS can be obtained in a matrix form as below.

$$\begin{bmatrix} \frac{2P_4\Omega_4 - \Omega_1^2}{\Omega_1} & 0 \\ 0 & \frac{2P_4\Omega_4 - \Omega_1^2}{\Omega_4} \end{bmatrix}\begin{bmatrix} \ddot{\theta}_2 \\ \ddot{x} \end{bmatrix} + \begin{bmatrix} \frac{4P_4\Omega_2 + 2P_4b_{fb} - \Omega_3\Omega_1}{\Omega_1} & -\frac{2P_4\Omega_3 + \Omega_1b_m}{\Omega_1} + \frac{k_tk_b}{R_mr^2} \\ -\frac{\Omega_3\Omega_4 - 2\Omega_1\Omega_2 - \Omega_1b_{fb}}{\Omega_4} & -\frac{b_m\Omega_4 + \Omega_3\Omega_1}{\Omega_4} + \frac{k_tk_b}{R_mr^2} \end{bmatrix}\begin{bmatrix} \dot{\theta}_2 \\ \dot{x} \end{bmatrix} + \begin{bmatrix} \frac{2P_4P_{10}'}{\Omega_1} \\ \frac{\Omega_1P_{10}'}{\Omega_4} \end{bmatrix} = \begin{bmatrix} \frac{k_tr}{R_mr^2} \\ \frac{k_tr}{R_mr^2} \end{bmatrix} V_{dc}. \tag{30}$$

The Eqs. (31)-(37) are introduced for further simplification of the FBCS equation in a matrix form.

$$\Omega_1 = P_5 + P_6D_1 + P_7D_2, \tag{31}$$

$$\Omega_2 = 2P_2D_1D_1' + 2P_3D_2D_2' + P_8P_9'D_1 + P_8P_9D_1', \tag{32}$$

$$\Omega_3 = P_6D_1' + P_7D_2', \tag{33}$$

$$\Omega_4 = 2P_1 + 2P_2D_1^2 + 2P_3D_2^2 + 2P_8P_9D_1, \tag{34}$$

$$D_1' = -\frac{l_2}{l_3(\theta_3 - \theta_4)} - \frac{l_2^2(\theta_2 - \theta_4)^2}{l_3^2(\theta_3 - \theta_4)^3} - \frac{l_2\left(\frac{l_2}{l_3(\theta_3 - \theta_4)} - \frac{l_2(\theta_2 - \theta_4)}{l_3(\theta_3 - \theta_4)^2}\right)(\theta_2 - \theta_3)}{l_4(\theta_3 - \theta_4)}, \tag{35}$$

$$D_2' = -\frac{l_2}{l_4(\theta_3 - \theta_4)} + \frac{l_2^2(\theta_2 - \theta_3)^2}{l_4^2(\theta_3 - \theta_4)^3} - \frac{l_2\left(\frac{l_2}{l_4(\theta_3 - \theta_4)} + \frac{l_2(\theta_2 - \theta_3)}{l_4(\theta_3 - \theta_4)^2}\right)(\theta_2 - \theta_4)}{l_3(\theta_3 - \theta_4)}, \tag{36}$$

$$P_{10}' = \frac{gl_2m_2}{2} + gl_2m_3 - \frac{gl_2m_3(\theta_2 - \theta_4)}{2(\theta_3 - \theta_4)} - \frac{gl_2m_4(\theta_2 - \theta_3)}{2(\theta_3 - \theta_4)}. \tag{37}$$

Although the resulting equation of motion is long due to the system containing a four-bar mechanism, it can be written in matrix form with the defined simplification terms. The simplification terms which contain $\theta_3$and θ_4 can be obtained depending on measured θ_2. The closed form of the equation of motion can be defined as follows:

$$\boldsymbol{M_{fb}}(\theta_2)\ddot{\boldsymbol{\rho}} + \boldsymbol{C_{fb}}\left(\theta_2, \dot{\theta}_2\right)\dot{\boldsymbol{\rho}} + \quad \boldsymbol{G_{fb}}(\theta_2) = \boldsymbol{F_{fb}}V_{dc}. \tag{38}$$

The above equation and the equation of motion of the IPCS defined in (6) have the same form. The notation $(\bullet)_{fb}$ is used as a subscript to associate the four-bar mechanism in the FBCS equation.

4. Lyapunov based backstepping controller

4.1. Controller design for inverted pendulum on a cart system

The dynamic equation of the IPCS given in (6) can be written by converting the following model to realize Lyapunov type backstepping controller [31].

$$\boldsymbol{M}(\theta)\dot{\boldsymbol{\nu}} + \boldsymbol{C}\left(\theta, \dot{\theta}\right)\boldsymbol{\nu} + \boldsymbol{G}(\theta) = \boldsymbol{F}V_{dc},$$

$$\dot{\boldsymbol{q}} = \boldsymbol{\nu}. \tag{39}$$

Here $\boldsymbol{q} = [x \quad \theta]^T$ is the system state of the IPCS. The position tracking error, $\tilde{\boldsymbol{q}} \in \mathbb{R}^{2\times1}$ and its time derivative $\tilde{\boldsymbol{\nu}} \in \mathbb{R}^{2\times1}$ can be defined as follows:

$$\tilde{\boldsymbol{q}} = \boldsymbol{q} - \boldsymbol{q_d},$$

$$\tilde{\boldsymbol{\nu}} = \boldsymbol{\nu} - \boldsymbol{\nu_d}. \tag{40}$$

Here $\boldsymbol{q_d}$ and $\boldsymbol{\nu_d}$ represent the desired position and velocity, respectively. To continue the implementation of the controller the virtual control signal can be defined as follows.

$$\dot{\boldsymbol{q}} = \boldsymbol{\nu} = \boldsymbol{s} + \boldsymbol{\alpha} \tag{41}$$

where $\boldsymbol{s} = \tilde{\boldsymbol{\nu}} + \boldsymbol{\Lambda}\tilde{\boldsymbol{q}}$ is the new state vector used for tracking control and $\boldsymbol{\alpha}$ is the stabilizing vector field can be chosen as

$$\boldsymbol{\alpha} = \boldsymbol{\nu_r} = \boldsymbol{\nu_d} - \boldsymbol{\Lambda}\tilde{\boldsymbol{q}} \tag{42}$$

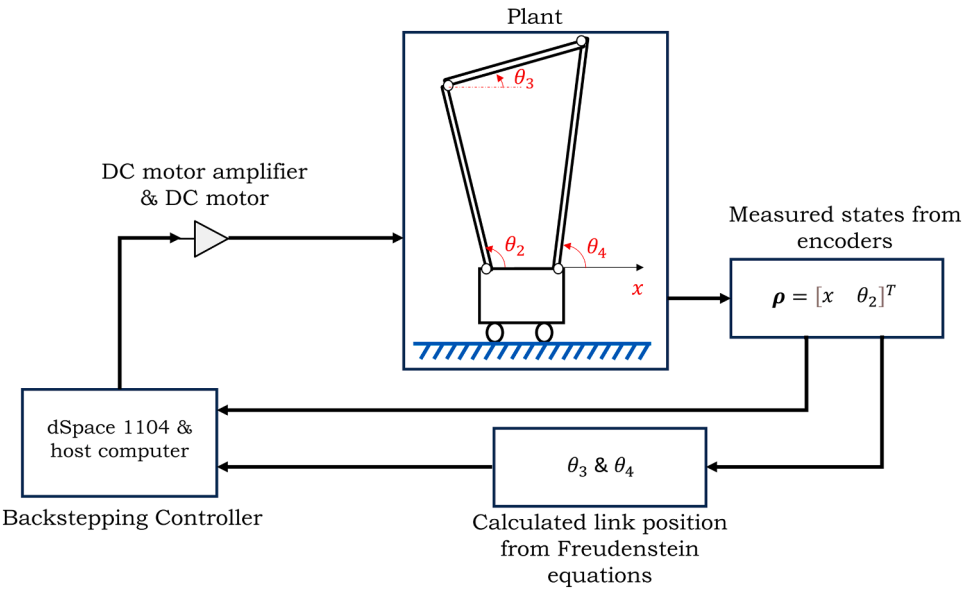

Fig. 5. Simplified block diagram of proposed FBCS controller.

where $\boldsymbol{\Lambda} \in \mathbb{R}^{2\times 2}$ positive-definite design matrix of the controller. In order to illustrate the candidate Lyapunov function, the position tracking error's (40) derivative can be expressed as following:

$$\dot{\tilde{\boldsymbol{q}}} = \boldsymbol{v} - \boldsymbol{v}_d = \boldsymbol{s} + \boldsymbol{\alpha} - \boldsymbol{v}_d = -\boldsymbol{\Lambda}\tilde{\boldsymbol{q}} + \boldsymbol{s}. \tag{43}$$

The configuration of the system Eq. (39) can be used to implement the backstepping design.

$$\boldsymbol{M}\dot{\boldsymbol{s}} + \boldsymbol{C}\boldsymbol{s} = \boldsymbol{F}V_{dc} - \boldsymbol{M}\dot{\boldsymbol{v}}_r - \boldsymbol{C}\boldsymbol{v}_r - \boldsymbol{G}. \tag{44}$$

The candidate Lyapunov function and its time derivative can be defined as follows:

$$V = \frac{1}{2}\tilde{\boldsymbol{q}}^T\boldsymbol{K}_p\tilde{\boldsymbol{q}} + \frac{1}{2}\boldsymbol{s}^T\boldsymbol{M}\boldsymbol{s},$$

$$\dot{V} = -\tilde{\boldsymbol{q}}^T\boldsymbol{K}_p\boldsymbol{\Lambda}\tilde{\boldsymbol{q}} + \boldsymbol{s}^T\boldsymbol{K}_p\tilde{\boldsymbol{q}} + \boldsymbol{s}^T\boldsymbol{M}\dot{\boldsymbol{s}}. \tag{45}$$

Where $\boldsymbol{K}_p \in \mathbb{R}^{2\times 2}$ is the positive-definite design matrix.

$$\boldsymbol{F}V_{dc} = \boldsymbol{M}\dot{\boldsymbol{v}}_r + \boldsymbol{C}\boldsymbol{v}_r + \boldsymbol{G} - \boldsymbol{K}_p\tilde{\boldsymbol{q}} - \boldsymbol{K}_d\boldsymbol{s} \tag{46}$$

where $\boldsymbol{K}_d \in \mathbb{R}^{2\times 2}$ is the positive-definite design matrix. The motor control voltage input V_{dc} obtained by the pseudeo-inverse of $\boldsymbol{F}^{\dagger} = \left(\boldsymbol{F}^T\boldsymbol{F}\right)^{-1}\boldsymbol{F}^T$. Finally, the negative-definite derivative of the Lyapunov function is obtained as:

Table 1
Parameters of the IPCS and FBCS.

Parameter	Definition	Value and unit
M	mass of the cart	0.669[kg]
m	mass of the pendulum rod	0.3 [kg]
l	pendulum length from pivot point to centre of gravity of the rod	0.25 [m]
J_p	mass moment of inertia of pendulum rod	0.008 [kgm^2]
b_{eq}	viscous friction coefficient for cart displacement	2.63 [Nms/m]
b_p	viscous friction coefficient for pendulum pivot point	0.6 [Nms/rad]
k_t	DC motor torque constant	0.01 [Nm/A]
r_m	DC motor pinion radius	0.018 [m]
k_b	DC motor back emf constant	0.01 [V/rad/sec]
R_m	DC motor armature resistance	35.2 [Ω]
g	acceleration of gravity	9.81 [m/s^2]
m_2	mass of the link−2 in four-bar mechanism	0.116 [kg]
m_3	mass of the link−3 in four-bar mechanism	0.079 [kg]
m_4	mass of the link−4 in four-bar mechanism	0.133 [kg]
l_1	length of the link−1 in four-bar mechanism	0.18 [m]
l_2	length of the link−2 in four-bar mechanism	0.415 [m]
l_3	length of the link−3 in four-bar mechanism	0.28 [m]
l_4	length of the link−4 in four-bar mechanism	0.48 [m]
I_2	mass moment of inertia of link−2 in four-bar mechanism	0.0017904 [kgm^2]
I_3	mass moment of inertia of link−3 in four-bar mechanism	0.0005811 [kgm^2]
I_4	mass moment of inertia of link−4 in four-bar mechanism	0.0027339 [kgm^2]
b_{fb}	viscous friction coefficient for four-bar mechanism joints	0.7 [Nms/rad]

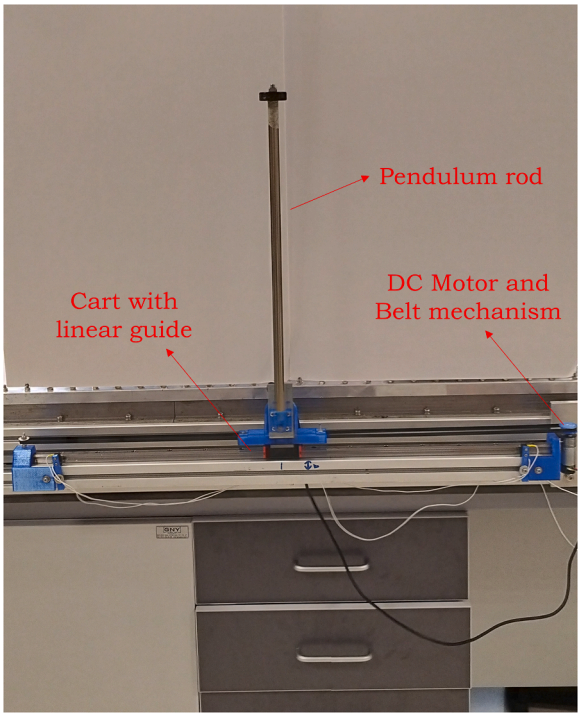

Fig. 6. Inverted pendulum on a cart experimental setup.

$$\dot{V} = -\boldsymbol{s}^T(\boldsymbol{C}+\boldsymbol{K}_d)\boldsymbol{s} - \tilde{\boldsymbol{q}}^T\boldsymbol{K}_p\boldsymbol{\Lambda}\tilde{\boldsymbol{q}}. \quad (47)$$

Given that V is positive definite and $\dot{V}$ is negative definite, then $(\tilde{\boldsymbol{q}}, \boldsymbol{s}) = (0,0)$ exponential stability is achieved globally.

4.2. Controller design for four-bar on a cart system

The equation of motion of the IPCS (6) and the equation of motion of the FBCS (38) share the same equational form. The state vector for the IPCS is denoted as $\boldsymbol{q} = [x \quad \theta]^T$, while the state vector for the FBCS is defined as $\boldsymbol{\rho} = [x \quad \theta_2]^T$. Since the Lyapunov-type Backstepping controller was designed in the previous section, equation of the controller can be similarly obtained for the FBCS which can be defined as following:

$$\boldsymbol{F}_{fb}V_{dc} = \boldsymbol{M}_{fb}\dot{\boldsymbol{v}}_r + \boldsymbol{C}_{fb}\boldsymbol{v}_r + \boldsymbol{G}_{fb} - \boldsymbol{K}_p\tilde{\boldsymbol{q}} - \boldsymbol{K}_d\boldsymbol{s}. \quad (48)$$

Fig. 5 illustrates the control block diagram structure applied to the proposed system. The key distinction here is that the dynamic matrices of the system are dependent on all angles of the four-bar mechanism (θ_2, θ_3, and θ_4), and the linear position of the cart (x). While x and θ_2 are measured using a two different encoder in the system, other variables of the four-bar mechanism are obtained through the Freudenstein equation.

5. Experimental studies

In this study, experiments were conducted using the same system for both the IPCS and the FBCS. Initially, experimental work was conducted for the classical inverted pendulum problem. Subsequently, the system was modified by substituting a four-bar mechanism for pendulum rod. Table 1 provides the physical parameters of both systems.

5.1. Experimental studies and results for inverted pendulum on a cart system

In Fig. 6, the experimental system of the IPCS is presented. In this system, an encoder and a pivot joint are positioned on the cart. The cart system is driven by a belt-pulley and a DC motor. The angular position of the pendulum rod, connected to the pivot joint, is measured in real-time through an incremental encoder. This information is then monitored on the host computer using the dSpace 1104 system. Similarly, another incremental encoder integrated into the DC motor shaft measures the linear position of the cart. Lyapunov type backstepping controller coefficients have been utilized for the in the IPCS as follows:

$$\boldsymbol{\Lambda} = \begin{bmatrix} 0.0025 & 0 \\ 0 & 0.0035 \end{bmatrix}, \boldsymbol{K}_p = \begin{bmatrix} 0.015 & 0 \\ 0 & 0.015 \end{bmatrix}$$

$$\boldsymbol{K}_d = \begin{bmatrix} 0.003 & 0 \\ 0 & 0.003 \end{bmatrix}. \quad (49)$$

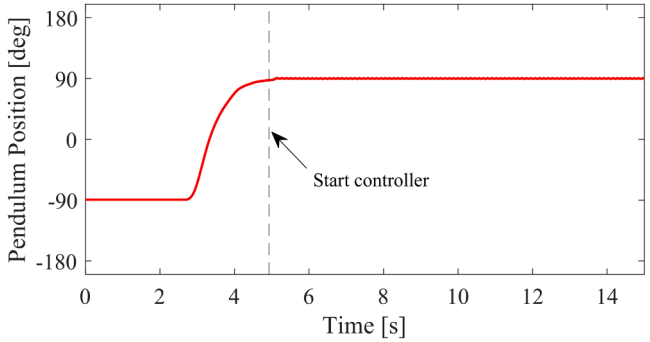

Fig. 7. Pendulum position for Backstepping controller.

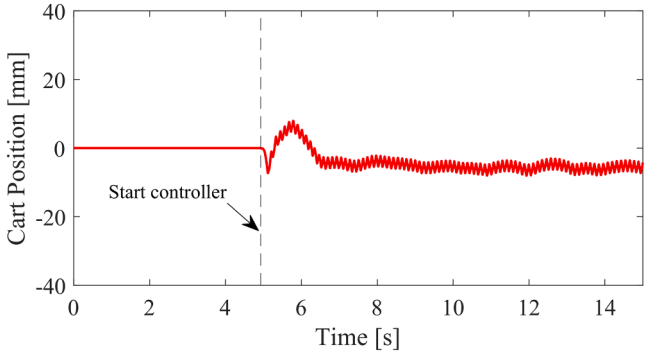

Fig. 8. Cart position for Backstepping controller.

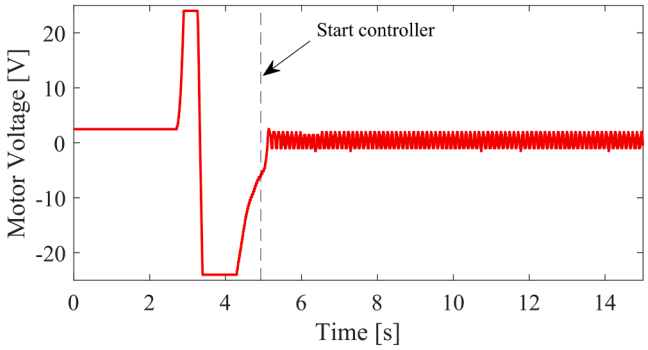

Fig. 9. IPCS motor control input.

The pendulum rod is initially at a lower position ($\theta = 270^0$) due to the effect of gravity. The controller is activated after maneuvering the pendulum rod around the equilibrium position. Fig. 7 shows the pendulum position for proposed Lyapunov type Backstepping controller with respect to time. Once the controller is activated (around 5 s indicated in Fig. 7), the cart is able to perform linear movements to preserve pendulum rod balance position. Fig. 8 shows the linear position of the cart. To keep the pendulum rod in a balanced position, the necessary linear motion of the car is achievable through a DC motor belt-pulley

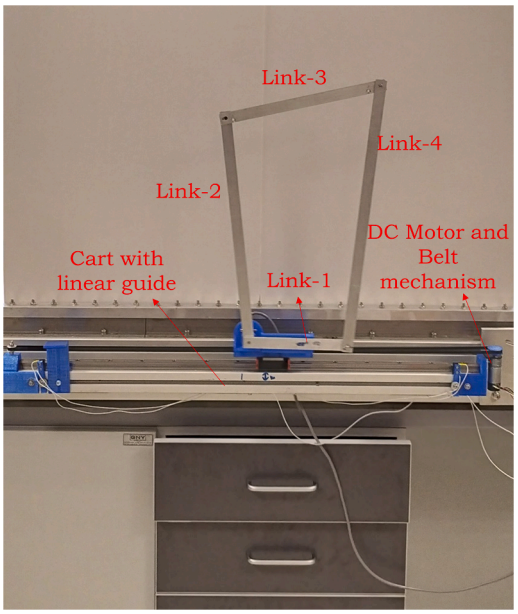

Fig. 10. Four-bar on a cart experimental setup.

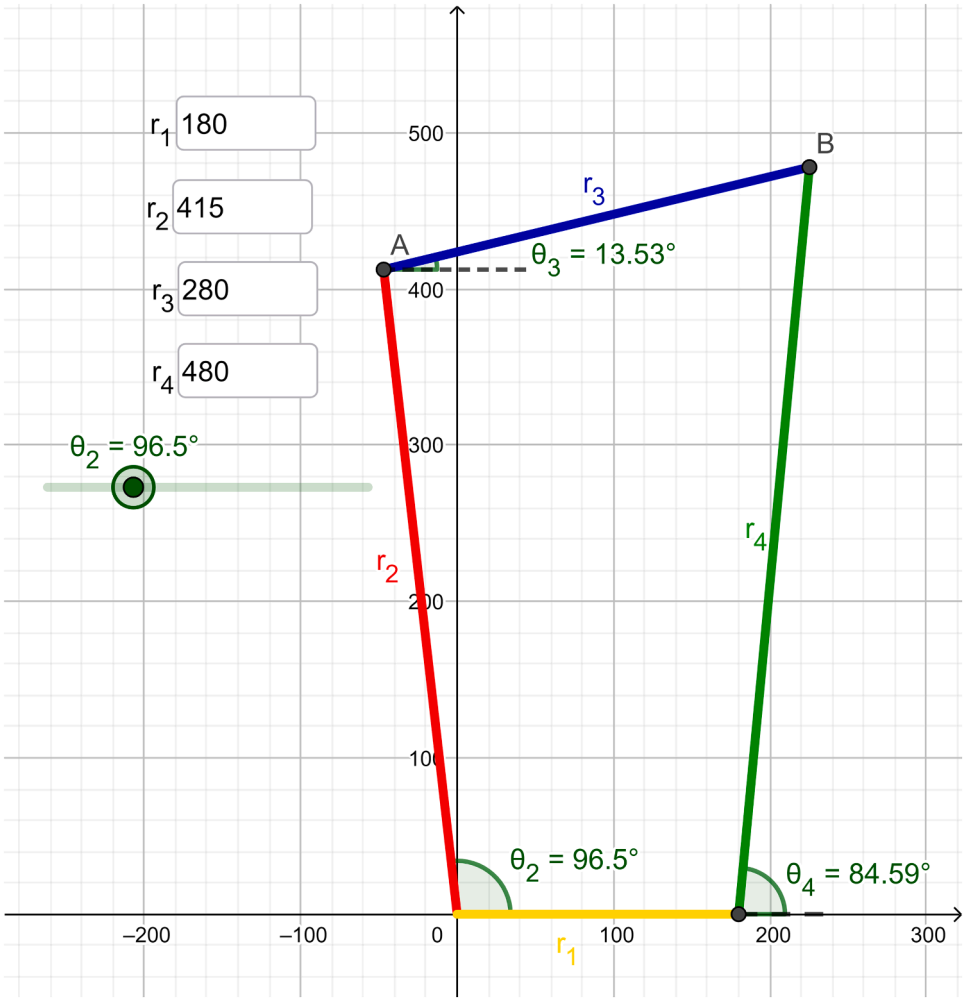

Fig. 11. Linkage synthesis of four-bar mechanism using GeoGebra at balance position.

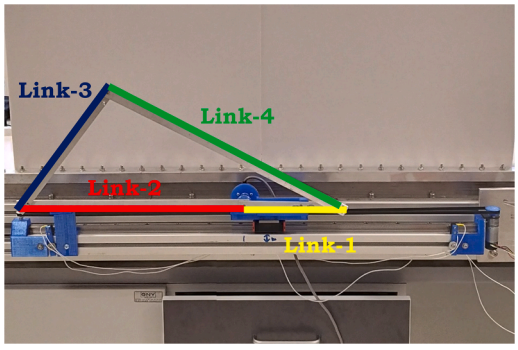

Fig. 12. Initial position of a four-bar mechanism.

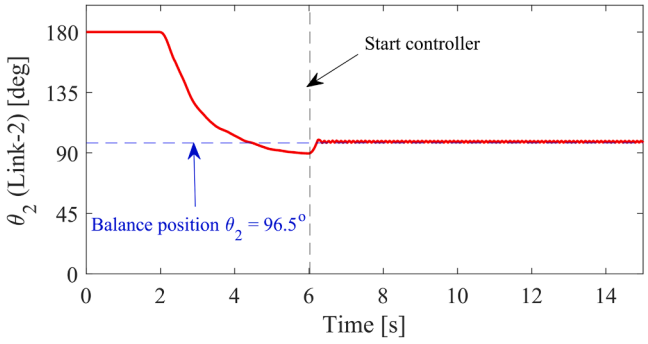

Fig. 13. Link-2 position for Backstepping controller.

system. The control input of the DC motor is calculated by the controller as shown in Fig. 9.

5.2. *Experimental studies and results for four-bar on a cart system*

In the experimental system, the pendulum rod has been replaced with a four-bar mechanism. In the mechanism, link-1 represents the fixed member. The position $\theta_2(t)$ can be measured with an encoder located at the hinge point of link-2. Fig. 10 shows the modified experimental setup. To ensure the stability of the four-bar mechanism, it is assumed that the line passing through the instant center of velocity point presented in Fig. 4 coincides with the line passing through the center of mass of the mechanism. Therefore, it has been determined that this position occurs when link-2 is at 96.5 degrees. The position analysis of the four-bar mechanism in this selected equilibrium state has been carried out using the GeoGebra program as shown in Fig. 11. In the four-bar mechanism, at the balanced position of link-3 is $\theta_3 = 13.53^{\circ}$, and link-4 is $\theta_4 = 84.59^{\circ}$. To keep this balance position for the Lyapunov type backstepping controller in the FBCS, the following control coefficients have been utilized.

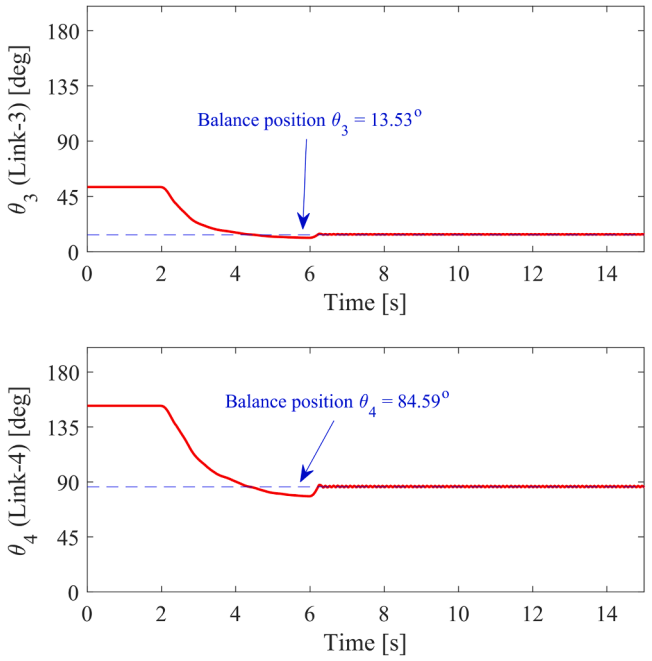

Fig. 14. Link-3 and link-4 position for Backstepping controller.

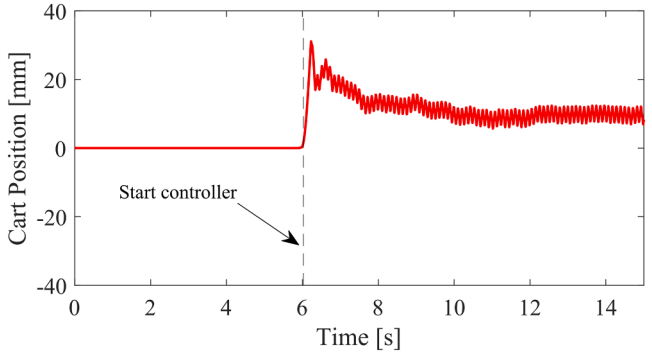

Fig. 15. Cart position FBCS for Backstepping controller.

$$\boldsymbol{\Lambda} = \begin{bmatrix} 0.0055 & 0 \\ 0 & 0.0065 \end{bmatrix}, \boldsymbol{K_p} = \begin{bmatrix} 0.015 & 0 \\ 0 & 0.015 \end{bmatrix},$$

$$\boldsymbol{K_d} = \begin{bmatrix} 0.003 & 0 \\ 0 & 0.003 \end{bmatrix}. \quad (50)$$

When the controller is disabled in FBCS, the mechanism has been positioned horizontally as shown in Fig. 12. Therefore, the initial angle of link-2 has been fixed at 180 degrees. This ensures that the incremental encoder used in the system reads a constant value at the beginning of the experiment. The initial positions of the mechanism $\theta_2(0)$, $\theta_3(0)$ and $\theta_4(0)$ are also can be seen in Figs. 13 and 14 at $t = 0$ s.

After the system is brought around to the equilibrium position from the initial position indicated in Fig. 12, the controller is activated via the host computer. As soon as the controller is activated, the system operates to maintain the four-bar mechanism in balance. Fig. 13 shows the angular displacement graph over time for link-2. The angular displacement information, calculated with the help of the Freudenstein equations, for link-2 and link-3 is presented in Fig. 14. The linear displacement of the cart over time is obtained when the equilibrium state is presented in Fig. 15. Finally, the motor control voltage calculated by the controller is presented in Fig. 16.

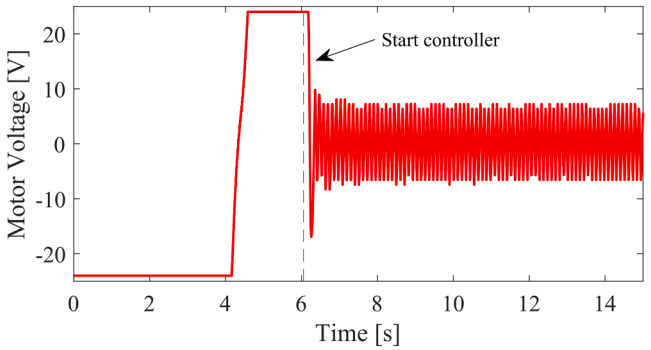

Fig. 16. FBCS motor control input.

6. Conclusion

In this study, the classic problem of the IPCS in automatic control theory has been approached with a different perspective. The four-bar mechanism, which forms the foundation of many machines, has been utilized in the system to maintain balance instead of the pendulum rod. The inverted pendulum system represents various applications, including the segway, balancing systems, rocket launches, structural system, and the simulation of human posture. Anything requiring vertical stabilization shares similar dynamics with the inverted pendulum system. On the other hand, the four-bar mechanism, in practice, emerges in various industrial fields such as compressors, motors, robotics, or mechatronic systems. As a result, it has been demonstrated in this study that a four-bar mechanism, having a similar degree of freedom, can be balanced on a moving car system.

By considering the dynamics of both the inverted pendulum system and the four-bar mechanism together, this study addresses a complex and multifaceted problem. One of the most challenging aspects of the mobile platform problem involving the four-bar mechanism is deriving the equations of the motion using the Lagrange method. This approach requires meticulous attention to the dynamic interactions and constraints within the system. However, the application of the Freudenstein equation significantly simplifies the process by allowing for the precise calculation of other variables based on the position of link-2 in the mechanism. This method not only enhances the accuracy of the model but also improves computational efficiency. The integration of these methodologies demonstrates a novel approach to solving balance and stabilization problems in dynamic systems. This innovative approach has the potential to be applied in various industrial and technological fields, offering improved performance and reliability in applications ranging from robotics to structural systems. Finally, in the proposed four-bar on cart system, as the lengths of the mechanism's links change, the system's center of mass and instant centers of velocity also change. Depending on the selection of the link dimensions, a four-bar mechanism can function as a crank-rocker, double-rocker, or double-crank mechanism. This means that the equilibrium position of the system will also change. As a future study, an investigation could be conducted to establish the correlation between the link lengths and the system's equilibrium position.

Funding

The author(s) received no financial support for the research, authorship, and/or publication of this article.

CRediT authorship contribution statement

Sinan Basaran: Writing – review & editing, Writing – original draft, Visualization, Software, Methodology, Investigation, Formal analysis, Data curation, Conceptualization.

Declaration of Competing Interest

The authors declare that they have no known competing financial interests or personal relationships that could have appeared to influence the work reported in this paper.

References

[1] Lee J, Mukherjee R, Khalil HK. Output feedback stabilization of inverted pendulum on a cart in the presence of uncertainties. Automatica 2015;54:146–57. https://doi.org/10.1016/J.AUTOMATICA.2015.01.013.

[2] Anderson CW. Learning to control an inverted pendulum using neural networks. IEEE Control Syst Mag 1989;9(3):31–7. https://doi.org/10.1109/37.24809.

[3] Boubaker O. The inverted pendulum benchmark in nonlinear control theory: A survey. London, England: SAGE PublicationsSage UK; 2013. https://doi.org/10.5772/55058.

[4] O. Boubaker, "The inverted pendulum: A fundamental benchmark in control theory and robotics," in International Conference on Education and e-Learning Innovations, 2012, pp. 1–6. doi: 10.1109/ICEELI.2012.6360606.

[5] S. Kajita and K. Tani, "Study of dynamic biped locomotion on rugged terrain-derivation and application of the linear inverted pendulum mode," in Proceedings. 1991 IEEE International Conference on Robotics and Automation, Los Alamitos, CA, USA: IEEE Computer Society, Apr. 1991, p. 1405,1406,1407,1408,1409,1410,1411. doi: 10.1109/ROBOT.1991.131811.

[6] T. Sugihara, Y. Nakamura, and H. Inoue, "Real-time humanoid motion generation through ZMP manipulation based on inverted pendulum control," in Proceedings 2002 IEEE International Conference on Robotics and Automation (Cat. No.02CH37292), 2002, pp. 1404–1409 vol.2. doi: 10.1109/ROBOT.2002.1014740.

[7] Pathak K, Franch J, Agrawal SK. Velocity and position control of a wheeled inverted pendulum by partial feedback linearization. IEEE Trans Robot 2005;21(3):505–13. https://doi.org/10.1109/TRO.2004.840905.

[8] Kim Y, Kim SH, Kwak YK. Dynamic analysis of a nonholonomic two-wheeled inverted pendulum robot. J Intell Robot Syst 2005;44(1):25–46. https://doi.org/10.1007/s10846-005-9022-4.

[9] Torres-Moreno JL, Cruz NC, Álvarez JD, Redondo JL, Giménez-Fernandez A. An open-source tool for path synthesis of four-bar mechanisms. Mech Mach Theory 2022;169:104604. https://doi.org/10.1016/j.mechmachtheory.2021.104604.

[10] Zhao J-S, Yan Z-F, Ye L. Design of planar four-bar linkage with n specified positions for a flapping wing robot. Mech Mach Theory 2014;82:33–55. https://doi.org/10.1016/j.mechmachtheory.2014.07.006.

[11] Aoustin Y, Hamon A. Human like trajectory generation for a biped robot with a four-bar linkage for the knees. Rob Auton Syst 2013;61(12):1717–25. https://doi.org/10.1016/j.robot.2013.06.002.

[12] Wahit MAA, Ahmad SA, Marhaban MH, Wada C, Izhar LI. 3d printed robot hand structure using four-bar linkage mechanism for prosthetic application. Sensors (Switzerland) 2020;20(15):1–22. https://doi.org/10.3390/s20154174.

[13] Franco E, Astolfi A, Rodriguez y Baena F. Robust balancing control of flexible inverted-pendulum systems. Mech Mach Theory 2018;130:539–51. https://doi.org/10.1016/J.MECHMACHTHEORY.2018.09.001.

[14] Huang J, Wang QG. Decentralized adaptive control of interconnected nonlinear systems with unknown control directions. ISA Trans 2018;74:60–6. https://doi.org/10.1016/j.isatra.2018.01.008.

[15] K.H. Lundberg and J.K. Roberge, "Classical dual-inverted-pendulum control," in 42nd IEEE International Conference on Decision and Control (IEEE Cat. No.03CH37475), 2003, pp. 4399-4404 vol.5. doi: 10.1109/CDC.2003.1272198.

[16] Tsai MC, Shen BH. Synchronisation control of parallel dual inverted pendulums driven by linear servomotors. IET Control Theory Appl 2007;1(1):320–7. https://doi.org/10.1049/iet-cta:20060038.

[17] Erkaya S, Uzmay I. Investigation on effect of joint clearance on dynamics of four-bar mechanism. Nonlinear Dyn 2009;58(1–2):179–98. https://doi.org/10.1007/s11071-009-9470-7.

[18] A. Ebrahim and G.V. Murphy, Adaptive backstepping controller design of an inverted pendulum, Proceedings of the Annual Southeastern Symposium on System Theory, vol. 37, pp. 172–174, 2005, doi: 10.1109/SSST.2005.1460900.

[19] Maruki Y, Kawano K, Suemitsu H, Matsuo T. Adaptive backstepping control of wheeled inverted pendulum with velocity estimator. Int J Control Autom Syst 2014;12(5):1040–8. https://doi.org/10.1007/s12555-013-0402-4.

[20] Das A, Lewis FL. Cooperative adaptive control for synchronization of second-order systems. Int J Robust Nonlinear Control 2010;18:557–69. https://doi.org/10.1002/rnc.

[21] Jmel I, Dimassi H, Hadj-Said S, M'Sahli F. An adaptive sliding mode observer for inverted pendulum under mass variation and disturbances with experimental validation. ISA Trans 2020;102:264–79. https://doi.org/10.1016/j.isatra.2020.02.029.

[22] Aguilar LT, Ortega JA, Ferreira A. Self-excited oscillations in an inverted cart–pendulum based on the two-relay approach. ISA Trans 2022;121:306–15. https://doi.org/10.1016/j.isatra.2021.04.015.

[23] Muškinja N, Tovornik B. Swinging up and stabilization of a real inverted pendulum. IEEE Trans Ind Electron 2006;53(2):631–9. https://doi.org/10.1109/TIE.2006.870667.

[24] M. Bugeja, Non-linear swing-up and stabilizing control of an inverted pendulum system, IEEE Region 8 EUROCON 2003: Computer as a Tool - Proceedings, vol. B, pp. 437–441, 2003, doi: 10.1109/EURCON.2003.1248235.

[25] Chung CC, Hauser J. Nonlinear control of a swinging pendulum. Automatica 1995;31(6):851–62. https://doi.org/10.1016/0005-1098(94)00148-C.

[26] Lin C, Wang Q-G, Lee TH, He Y. Design of Observer-Based H_∞ Control for Fuzzy Time-Delay Systems. IEEE Trans Fuzzy Syst 2008;16(2):534–43. https://doi.org/10.1109/TFUZZ.2006.889934.

[27] Norton RL. Design of machinery an introduction to the synthesis and analysis of mechanisms and machines. Maidenhead: McGraw-Hill; 1999.

[28] Söylemez E. Correlation of Input and Output Motion; Function Generation; Freudenstein's Equation in Mechanism Design. Kinematic Synthesis of Mechanisms: Using Excel® and Geogebra. Cham: Springer Nature Switzerland; 2023. p. 333–99. https://doi.org/10.1007/978-3-031-30955-7_8.

[29] J.R. Chagdes, J.P. Freire, and A. Shukla, Nonlinear Dynamics of Upright Human Balance While Using a Passive-Cane, in Dynamic Systems and Control Conference, 2016, p. V001T10A005.

[30] S.A. Mohseni, V. Duchaine, and T. Wong, A comparative study of the optimal control design using evolutionary algorithms: Application on a close-loop system, 2017 Intelligent Systems Conference, IntelliSys 2017, vol. 2018-Janua, no. September, pp. 942–948, 2017, doi: 10.1109/IntelliSys.2017.8324243.

[31] Godhavn JM, Fossen TI, Berge SP. Non-linear and adaptive backstepping designs for tracking control of ships. Int J Adapt Control Signal Process 1998;12(8):649–70. https://doi.org/10.1002/(SICI)1099-1115(199812)12:8< 649::AID-ACS515> 3.0.CO;2-P.